

VII. MICROWAVE AND MILLIMETER WAVE TECHNIQUES

Academic and Research Staff

Prof. Bernard F. Burke	Prof. Robert L. Kyhl	Prof. David H. Staelin
Prof. Madhu S. Gupta	Prof. Paul L. Penfield, Jr.	Dr. Alan Parrish

Graduate Students

John Cooley	Thomas S. Giuffrida	Gary K. Montress
Patrick C. Crane	Lance A. Glasser	Robert C. Walker
	Aubrey D. Haschick	

A. FABRICATION AND CHARACTERISTICS OF MICROWAVE BARITT DIODES

JSEP

Joint Services Electronics Program (Contract DAAB07-75-C-1346)

Gary K. Montress, Madhu S. Gupta

Recent improvement in measurement accuracy for the slotted-line system used in all admittance measurements allows more accurate determination of package parasitics. We are now using a five-element equivalent-circuit model, rather than the four-element equivalent-circuit model reported in RLE Progress Report No. 117 (pp. 25-26). Figure VII-1 shows the new equivalent-circuit model for package parasitics composed of a single lead-wire connection (0.001" diam) and a double lead-wire connection (0.001" diam). The new model is highly accurate for representing package parasitics in the 4-8 GHz frequency range, which is the frequency range of interest in this work. This five-element equivalent circuit for package parasitics is used to de-embed the terminal admittance measurements on BARITT diodes back to the diode chip reference plane. A FORTRAN IV program has been written to accomplish the de-embedding.

The equivalent circuit proposed to fit the experimentally measured small-signal admittance of the BARITT diode, as shown in Fig. VII-2, incorporates only frequency-independent elements. These elements, however, will be bias-dependent and RF voltage level-dependent. In order to fit the model to the measured admittance data, accurate measurements of the admittance are required, for which standard slotted-line techniques are inadequate. The technique described by Bandler¹ has been modified slightly and is being used with good results. Our system differs from Bandler's, in that the RF test signal is introduced at one port of the slotted line instead of being coupled in through the moving probe. This permits independent measurement of the RF voltage across the BARITT diode. Thus the system is useful for both small-signal and large-signal measurement of admittance. Superheterodyne detection is used in both cases. With this technique accurate measurement of both VSWR and nodal shift data as a function of frequency, bias, and RF voltage level can be made. This is essential because the magnitude of the negative conductance in the BARITT diode is only a few ohms.

JSEP

(VII. MICROWAVE AND MILLIMETER WAVE TECHNIQUES)

JSEP

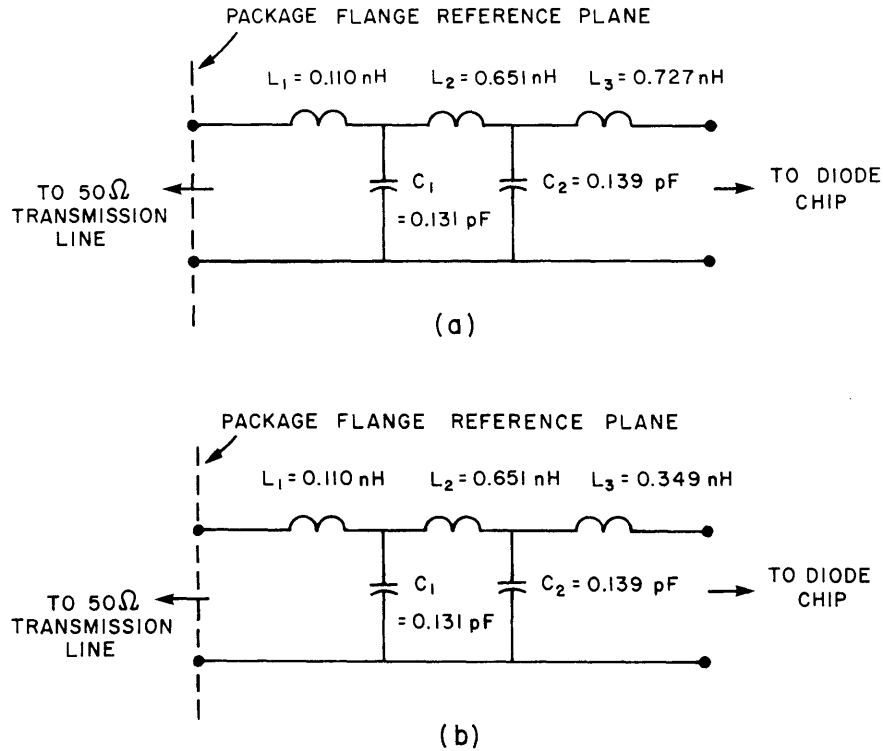


Fig. VII-1. Model for diode package parasitics. (a) One-wire lead. (b) Two-wire lead.

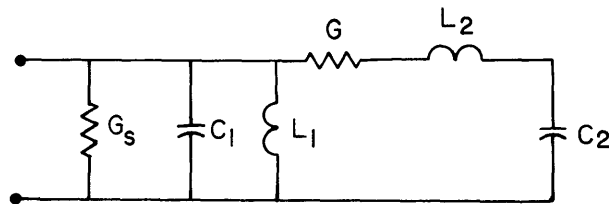


Fig. VII-2. Proposed circuit for representing BARITT diode terminal admittance.

We have measured the conductance and susceptance of a typical fabricated BARITT diode between 4.6 GHz and 7.8 GHz. The frequency range over which the device is active is approximately 5.2 GHz to 7.4 GHz. The proposed small-signal model for the BARITT diode does not fit the measured conductance and susceptance data over the full negative conductance passband. Hence the equivalent-circuit model proposed for the BARITT diode is used to fit the measured admittance data over a somewhat narrower band of frequency. For most of the diodes tested this frequency range is 5.6-6.8 GHz.

JSEP

amplifier or as a source. Figure VII-3 shows the result of a least-mean-square fit of the device model to the measured admittance data. At the operating point shown, $I_{dc} = 25.0$ mA, the values of the elements in the model are as follows: $G_s = 0.93 \times 10^{-4}$ mho, $G = -10.7 \times 10^{-4}$ mho, $C_1 = 0.616$ pF, $L_1 = 4.50$ nH, $C_2 = 0.0085$ pF, and $L_2 = 73.43$ nH. The maximum error of fit is 2% or less across the 5.6-6.8 GHz frequency range.

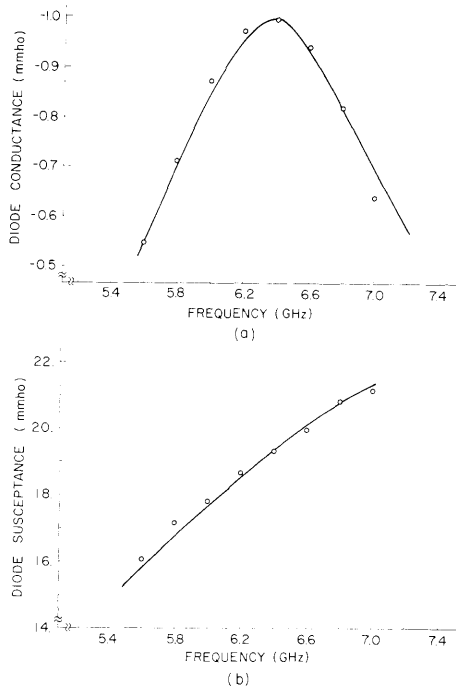


Fig. VII-3.

BARITT diode #1-h24171-B6-10 conductance and susceptance as a function of frequency. $I_{bias} = 25.0$ mA.

- (a) Equivalent-circuit conductance.
 (b) Equivalent-circuit susceptance.

The large-signal admittance of the device has been measured. The dependence of the device conductance G upon the RF voltage level may be modeled reasonably well by a functional dependence of the form $G(V_{RF}) = -G_o(1 - a_o V_{RF}^2)$. At the accuracy of the measurement system, the susceptance of the diode has been found to be RF voltage level-independent. Initial indications are that the small-signal model may be used to represent the large-signal behavior of the conductance; the conductances G_s and G are the only elements in the model that depend upon the RF voltage level.

Measurements of the device admittance at several values of the dc bias current I_{dc} have been made in the active region of the device. The results will be used again to fit the proposed diode model to the measurements, and to determine the bias dependence of the various elements in the model.

Other measurements, including FM sensitivity, are also being carried out to characterize the BARITT diode. We plan to relate these measurements to the admittance measurements and the proposed model for the BARITT diode.

1. J. W. Bandler, "Precision Microwave Measurement of the Internal Parasitics of Gunn Diodes," IEEE Trans. on Electron Devices, Vol. ED-15, No. 5, pp. 275-282, May 1968.

B. MICROWAVE MEASUREMENTS ON THE SILICON CRYOSAR

Joint Services Electronics Program (Contract DAAB07-75-C-1346)

Robert L. Kyhl, Lance A. Glasser

This is the final report on our study of the microwave properties of the silicon $n^+ - \nu - n^+$ cryogenic diode (cryosar). The cryosar is a three-region semiconductor diode that displays nonlinear characteristics only at liquid helium temperatures. It is composed of an intrinsic region sandwiched between two degenerately doped regions. All three regions must be of the same type, that is, $n^+ - \nu - n^+$ or $p^+ - \pi - p^+$. At room temperature this device is a resistor, but at cryogenic temperatures the carriers in the intrinsic region freeze out and the device looks like a capacitor. Application of a moderate voltage produces ionization of the residual donors in the ν region and current flows. This is an avalanche process. Although the cryosar was described¹ in 1959, we believe that this is the first report of microwave measurements, and that this is the first such device with a sufficiently thin ν region that transit times are small at microwave frequencies.

The fabrication of the microwave cryosars for this project was performed primarily in our microelectronics laboratory by Edward D. Nowak and Lance A. Glasser. Both planar- and mesa-type structures were tried with satisfactory results, but most of the measurements were performed on the mesa-type devices because they were easier to fabricate. Figure VII-4 shows a mesa-type cryosar.

We found that by making the intrinsic region of the silicon cryosar narrow ($\sim 1 \mu\text{m}$), breakdown fields of 10^5 V/m or greater could be achieved. This is two orders of magnitude higher than previously reported. We also found that even if differential negative resistance is present at dc (see Fig. VII-5 for a typical V-I plot), it is not necessarily

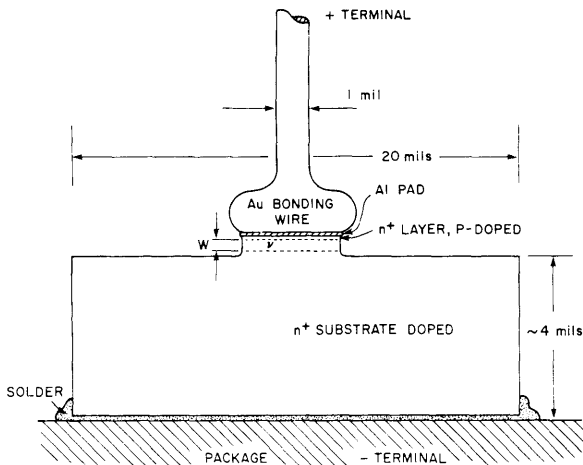


Fig. VII-4.

Microwave cryosar diode (not to scale).

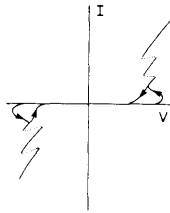


Fig. VII-5. V-I curve of a typical cryosar.

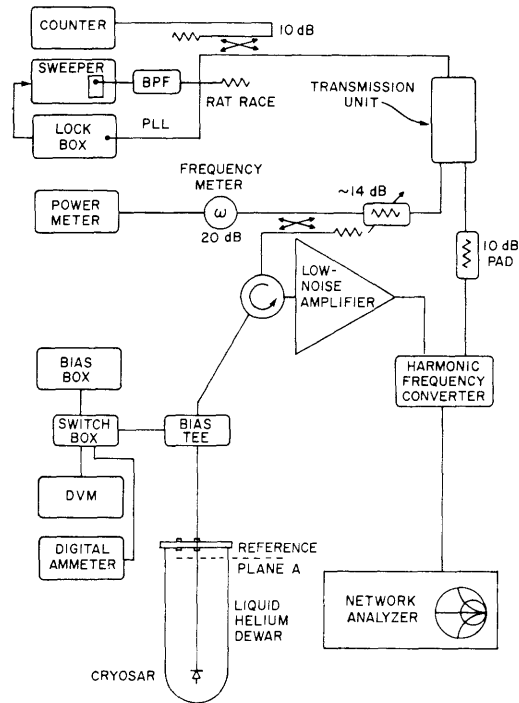


Fig. VII-6. Small-signal impedance measurement system.

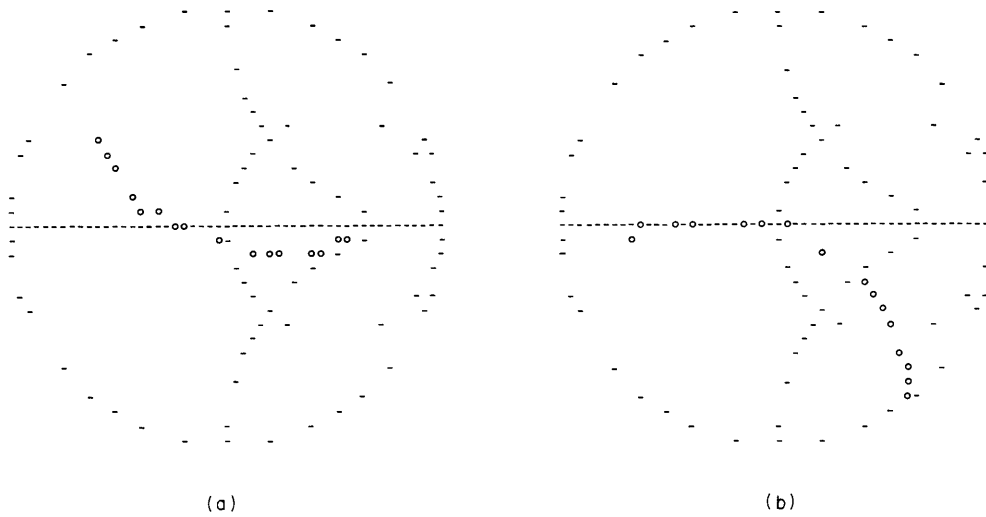


Fig. VII-7. Cryosar data at 1.3 GHz and +V biases: (a) before de-embedding; (b) after computer reduction.

(VII. MICROWAVE AND MILLIMETER WAVE TECHNIQUES)

JSEP

present at microwave frequencies (we never observed RF negative resistance).

The results of the microwave measurements follow.

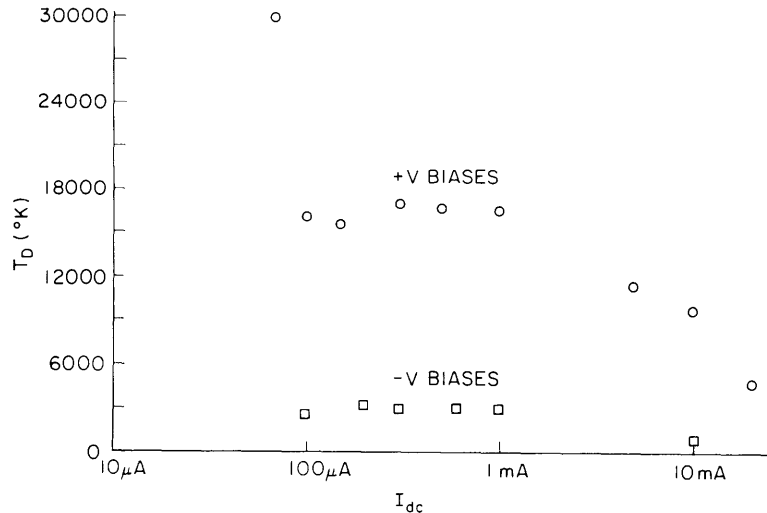
1. Small-Signal Impedance

For this work an HP network analyzer was enhanced so that it could operate with a signal power of less than $0.1 \mu\text{W}$ (Fig. VII-6). In order to refer the measurements to the terminals of the diode, de-embedding procedures must be applied, requiring three or more calibrated loads in place of the diode. We used MOS capacitors for this purpose, which, we believe, is an original approach to the problem. These experiments were done at 1.3 GHz and 3.0 GHz. Figure VII-7a is a Smith Chart plot of the small-signal impedance of the diode as a function of dc bias current at 1.3 GHz before de-embedding and Fig. VII-7b is a plot after the data had been reduced by computer. The departure of Fig. VII-7b from a parallel RC model at low and moderate currents can be interpreted as a phase lag in the avalanche current that would correspond to a time constant of a fraction of a nanosecond.

2. Qualitative Mixing Experiments

With large-signal drive at 1.3 GHz harmonic generation was observed up to at least 8 GHz.

Mixing was demonstrated up to 4 GHz. Since there are breaks in the V-I curve at both positive and negative voltages, it is possible to demonstrate harmonic mixing with the signal at 4 GHz and the local oscillator at 2 GHz. No measurements of conversion loss are available.



JSEP

Fig. VII-8. Cryosar diode noise temperature as a function of bias current.

3. Noise Temperature

The noise temperature of the diode was measured as a function of bias current with a 1.3 GHz radiometer. These data were corrected for additional noise sources and impedance mismatches. The results are plotted in Fig. VII-8. By standard avalanche diode noise theory² these data correspond to multiplication factors of 4.1 and 2.3 for the forward and reverse biases, respectively.

Detailed results are given in the Master's thesis of Lance A. Glasser, to be submitted to the Department of Electrical Engineering and Computer Science, M. I. T.

References

1. A. L. McWhorter and R. H. Rediker, "The Cryosar - A New Low-Temperature Computer Component," Proc. IRE 41, 1207-1213 (1959).
2. S. M. Sze, Physics of Semiconductor Devices (Wiley-Interscience, New York, 1969), pp. 675-683.

C. ATMOSPHERIC REFRACTION AT MILLIMETER WAVELENGTHS

Joint Services Electronics Program (Contract DAAB07-75-C-1346)

Bernard F. Burke, Alan Parrish, Thomas S. Giuffrida,
Aubrey D. Haschick

The development of the M. I. T. microwave interferometer continues, with emphasis on achieving a high degree of phase and delay stability in the completed instrument. The ultimate goal is to measure atmospheric refraction and absorption effects with high precision, especially at low elevation angles. Components of the instrument are now being tested in the laboratory in order to find and eliminate instrumental systematic effects. We plan a laboratory test of a complete two-element interferometer before the system is installed on the antennas. The phase stability of the instrument depends principally upon the performance of the local-oscillator system shown in Fig. VII-9. The measured environmental coefficients of the system are listed in Table VII-1. These measurements indicate an instrumental rms phase error of 3.5° corresponding to a path difference of 0.13 mm, or an angular accuracy of 0.07 arc-sec at the first observing wavelength, 13 mm.

A prototype of the delay and correlator system is now being tested in the laboratory. This device, using emitter-coupled logic, is clocked at 150 MHz, and has correlated noise signals with frequencies as high as 70 MHz. The detailed system engineering is nearly complete, with emphasis placed on achieving high reliability over long integration times.

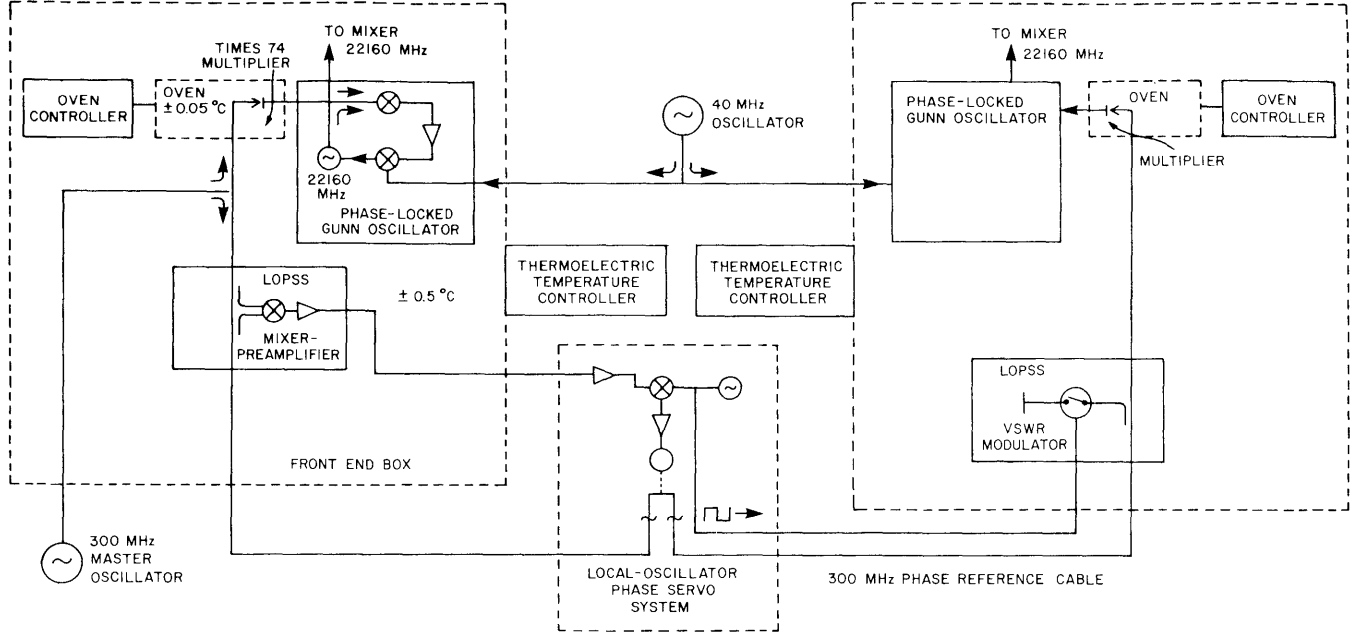


Fig. VII-9. Local oscillator system.

Table VII-1. Local oscillator system phase stability.

<u>Component</u>	<u>Environmental Condition</u>	<u>Expected Range of Condition</u>	<u>Error Coefficient</u>	<u>Expected Error</u>	<u>Notes</u>
Local Oscillator Phase Servo System (LOPSS) mixer preamplifier	Temperature	1°C	-2.6 ^{deg} /°C	-2.6°	1
LOPSS SWR modulator	Temperature	1°C	+1.3 ^{deg} /°C	+1.3°	1
LOPSS mixer preamplifier	300 MHz drive level	0.1 dB	5.5 ^{deg} /dB	0.6°	
LOPSS SWR modulator	300 MHz drive level	0.1 dB	negligible	—	
LOPSS	Reference cable length	1 cm	0.3 ^{deg} /cm	0.3°	
300-22200 MHz multiplier	Temperature	0.1°C	10 ^{deg} /°C	1°	2
Gunn oscillator and lock loop	Temperature	1°C	negligible	—	

Notes.

1. Controlled by radiometer temperature controller.
2. Controlled by proportionally controlled oven.

(VII. MICROWAVE AND MILLIMETER WAVE TECHNIQUES)

JSEP

The three receiver front ends have been completed, and all underground cabling has been installed. The drives, controls, and wiring are finished on two antennas and half-finished on the third. The first radiometer temperature control system is now being tested in the laboratory, and construction of the other two is in progress.

Interferometer observations are scheduled to start this summer. Initial observations will begin at 13 mm wavelength, and atmospheric refraction and absorption will be measured under all weather conditions, and over a wide range of elevation angles. Measurements will be made at the lowest elevation angles permitted by atmospheric absorption.

Work has begun on planning the next stage of the interferometer, a 7-mm system that will utilize cooled mixers. The first radiometer will be used to evaluate the antenna gain of the 18 ft paraboloids, and two-element interferometer measurements should be made soon thereafter.

JSEP